JOURNAL OF MATERIALS SCIENCE **39** (2004) 1195–1205

Density analysis of direct metal laser re-melted 316L stainless steel cubic primitives

R. MORGAN, C. J. SUTCLIFFE, W. O'NEILL
Manufacturing Science and Engineering Research Centre, Department of Engineering, The University of Liverpool, UK
E-mail: rhm32@cam.ac.uk

This paper reports on the density of cubic primitives made by Direct Metal Laser Re-Melting, a process variant of selective laser sintering (SLS). Here, stainless steel 316L powder fractions are scanned and fused by a 90 W Nd:YAG laser in consecutive 100 μm layers in order to build a 3-Dimensional object. The effects of Q-Switch pulsing frequency, scanning speed and scan spacing on sample density are described. The samples are measured by two methods: a weight/volume analysis and a xylene impregnation technique. The results are supported by microscopy analysis for qualitative arguments. The results show the significant influence of pulsing the beam on the density of the fabricated material. Also reported is the relationship of material density with energy density (as a function of the process parameters; power, scan speed and scan spacing). Optical analysis of material cross sections shows a periodic occurrence of porosity across the whole range of samples. Causes for this are discussed.

1. Introduction

Powder based rapid prototyping (RP) processes such as selective laser sintering (SLS) enable the production of complex 3-D objects in a wide variety of materials and in reduced time, thus shortening the design process and generating cost and time savings. In the SLS process, a three dimensional computer aided design (CAD) model is sliced into many horizontal layers. The first layer is created by scanning an infra-red laser beam across the surface of a powder bed, which selectively heats, melts and bonds only the powder that corresponds to the particular cross section of the CAD model. When the layer is complete, the powder bed lowers by a single layer thickness (typically 100 μm) by means of a piston. A fresh layer of loose powder is deposited over the bed by means of a roller or scraper and the process is repeated. When all layers are complete, the piston is raised, the object removed from the bed and excess powder is removed.

Automated, layered manufacturing processes such as SLS and Stereolithography (SLA) are now also used for Rapid Tooling and Rapid Manufacturing of components, further reducing time-to-market and competing with traditional tooling/production processes per unit cost depending on part dimensions [1]. The production of functional, load bearing metallic objects by these routes, however, requires considerable development. Processes such as Indirect Metal Sintering utilise a low power laser to melt and bond a polymer binder component to act as a matrix in which metallic particles sit. This requires downstream processes to remove the binder and infiltrate the porous structure with a low melt temperature alloy for densification. Binary phase sintering processes such as direct metal laser sintering (DMLS) utilise the low temperature alloy powder directly as the binding component in a steel composite powder blend. Both routes, although successful in creating short and mid-run injection molding tooling, produce objects which are compromised by the strength of the lower melting point alloys. In order for SLS components to exhibit the same or similar physical properties as conventionally processed materials, the high temperature, high strength particles require processing without additional binders or infiltrants. This therefore requires the direct melting, fusion and resolidification of the material to form solid high density components.

There are, however, many barriers preventing the successful production of high-density components by this route. These include the large thermal stresses generated in the material due to steep thermal gradients imposed on the material by the scanning laser resulting in component distortion [2], but a more significant problem is oxidation resulting in reduced material wetting. As the SLS process is a layered technology, reduced wetting is a severe impediment to intra-laminar fusion and causes defects such as porosity, balling and delamination due to surface tension effects. The spherical shaping of the melt (due to a natural tendency of the surface free energy to minimise its area) may also be exacerbated by convective currents within the melt pool (Marangoni stirring), recognised as an impediment in laser welding processes [3].

Research within the Manufacturing Science and Engineering Research Centre, University of Liverpool aims to overcome these problems by investigating the effect of Q-switch laser pulse frequency on the

re-distribution of the melt in order to overcome the forces (surface tension and Marangoni) that are thought to contribute to the balling effect observed during DMLR and SLS processes. During pulsed mode, the radiation is incident on the material surface for short timescales. The low energy pulses, emitted over a short duration, typically nanoseconds, generate intense peak power densities of the order of $GWcm^{-2}$ [4]. The resulting effect on the material is instantaneous melting, vaporisation and ionisation of the fast expanding gas. The subsequent absorption of the laser energy by the plasma generates a heat-sustained shock wave that moves radially outwards from the interaction site. The high-pressure region immediately behind the shock wave exerts a large compressive force on the material, known as the evaporation recoil force. This compressive force has been shown by the author to result in a modification of the melt pool shape, resulting in increased material density during single layer DMLR studies [5].

This paper examines the effect of Q-Switch pulsing and the related recoil compression force on the density of multiple layer cubic primitives.

2. Experimental arrangement

The test facility for the DMLR process consists of a Rofin Sinar 90 W, Flash Lamp pumped, Q-switched Nd:YAG laser. The Nd:YAG laser was chosen over CO_2 laser due to increased absorption of a 1.064 μm wavelength by metallic powder compared to a larger 10.64 μm wavelength [3]. The Q-Switch enables pulse repetition rates of 0–60 kHz where 0 kHz is Continuous Wave (CW) mode. Pulse energies and pulse widths are in the range 1–30 mJ and 80–200 ns respectively. Maximum output power is measured as 80 W with a minimum beam diameter of 100 μm. Scan speeds up to 500 mm/s are achievable over 80 mm^2 square area by use of integrated galvanometer scanning mirrors.

The process apparatus consists of a powder feed cylinder and build cylinder arrangement housed in an atmospheric control chamber capable of evacuation of and purge with inert gas. Pistons in the cylinders are driven by 2 linear stepping actuators with minimum step size of 0.25 μm. Powder delivery is achieved by traversing powder from the feed cylinder to the build cylinder through use of a counter-rotating roller. All motors are controlled through in-house software, which also enables communication between laser and chamber to provide full automation of the process. Fig. 1 shows a schematic of the experimental arrangement.

Gas atomised, austenitic stainless steel 316L was used during the study. The powder is generally spherical in form and has a wide distribution. Particle diameters were in the range <1–56 μm with 80% <22 μm. The elemental composition of the alloy powder is: 16.73Cr, 13.19Ni, 0.017C, 0.71Si, 2.69Mo, 1.69Mn, Fe bal. In process loose powder bed density was calculated by mass/volume measurement. Three measurements of powder bed density were taken with the average density being recorded as 48% of theoretical density taken from reference text [6].

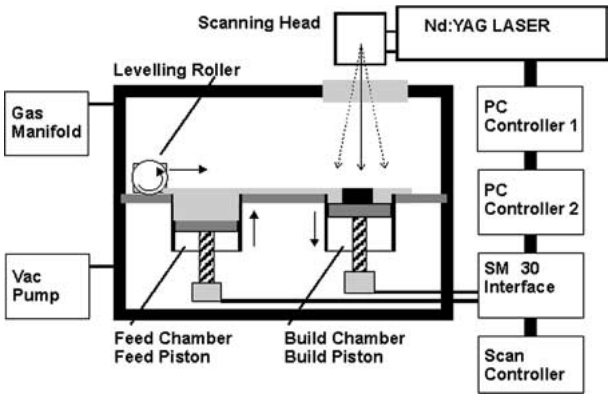

Figure 1 System schematic of experimental arrangement.

3. Experimental procedure

3.1. Cube fabrication

An experimental investigation of laser remelting of single layers on a loose powder bed showed evidence of curl (due to high thermal stresses generated by steep thermal gradients) and of protrusion of the initial scan lines of the layer due to a phenomenon called 'First Line Scan (FLS) Balling' [5]. The latter effect is due to the significant increase in absorbed energy from the incident beam during the initial rasterscan compared with the subsequent scans. As the laser scans over the powder, capillary forces induced by the wetting molten liquid cause a large volume of melt to be produced. During the second pass, only a portion of the beam is incident on the powder due to the overlap with the previous scan line. This results in a reduction of the melt volume and limited protrusion from the surface. The detrimental effects of material curl and first line protrusion cause movement of the underlying layer when depositing powder for the proceeding layer. In order to prevent FLS balling and anchor the layers to prevent curl, a 3 mm stainless steel 316L plate was employed to anchor the fused powder layers. This technique is employed in blown powder freeform fabrication processes such as LENS (Laser Engineered Net Shaping), and has also been used by other researchers for the pre-placed metal Selective Laser Powder Remelting (SLPR) where the substrate may be incorporated into the finished part [7].

Cubes were produced with the parameters listed in Table I. Power was kept at a maximum, measured at 80 W from the scanning head. Layer thickness was set at 100 μm. Nitrogen shroud gas was used for protection of the process from the atmosphere. Katayama showed this gas to reduce porosity in laser welding [8]. The beam diameter was set at 100 μm. A series of seven cubes were built during a single run, each cube produced at varying Q-switch Pulse Repetition Frequency

TABLE I Parameters examined for production of cubic primitives

Parameter	Values examined
Power (W)	80
Scan speed (mms^{-1})	50, 100, 200, 300, 400, 500
Scan spacing (μm)	25, 50, 75
Pulse frequency (kHz)	CW (0), 10, 20, 30, 40, 50, 60

(PRF). Scan spacing and scan speed remained constant during a single experiment. Scan spacing is defined as the distance between consecutive lines scanned by the laser. The scan spacing is generally a fraction of the beam diameter to ensure overlap between successive scan tracks. The cubes were produced with a bi-directional rasterscan pattern.

3.2. Density measurements

Cube densities were measured by two techniques, the first a simple mass/volume measurement using Oertling RB300 digital balance and Digital Mitutoyo vernier callipers (500-171 absolute digimatic). The second measurement was a porosity analysis by way of a xylene impregnation technique [9]. With this method, a series of weight measurements is taken. The cubes are first weighed in air and then are immersed in xylene and placed under a vacuum for one hour to remove the air from the open pores and allow the xylene to enter. The specimens are removed from the xylene and after removing surface liquid (by means of filter paper) are weighed in air and water. Xylene, being non-miscible with water, prevents the water from entering so that the difference between the last two weightings gives the total volume of the specimen. As the density of the xylene and stainless steel are known values, the interconnected, closed and total porosities can be calculated. The results of density are presented as a percent value of the theoretical material density given in the reference text.

3.3. Optical analysis

The samples were sectioned along the scan direction and normal to the scan direction, in order to evaluate any directionality of the porosity. The cubes were sectioned along the laser scanning direction and normal to the scan direction to observe variations in powder re-melting with respect to scan direction. The specimens were analyzed by standard metallographic techniques and observed under a high magnification optical microscope.

4. Results

4.1. Density measurements

Fig. 2 shows a typical set of cubes produced in a single experiment. Fig. 3a–c show the density of the cubes at varying scan speeds and pulse frequencies, analysed by weight/volume measurements and xylene impregnation technique. The two methods of measurement of density show good correlation with the xylene impregnation technique showing approximately 7.5% increase in measurements. The higher accuracy of xylene method has been previously demonstrated by Arthur [9].

The results show a general trend of increasing part density with decreasing scan speed. The effect of pulse frequency on the resulting density is significant and varied depending on the combination of process parameters used. Scan spacing does not have such a significant effect, but the general trend is a decrease in material density with decreasing scan spacing. The sample exhibiting the highest density was produced at CW mode, 100 mms^{-1} 75 μm scan spacing, measuring 87% of theoretical density.

At low scan speeds (100–200 mms^{-1}), samples produced in continuous wave (CW) mode and at high PRF (50–60 kHz) exhibited the highest densities. Within this low speed regime, material density is reduced slightly with decreasing PRF, with a much greater reduction

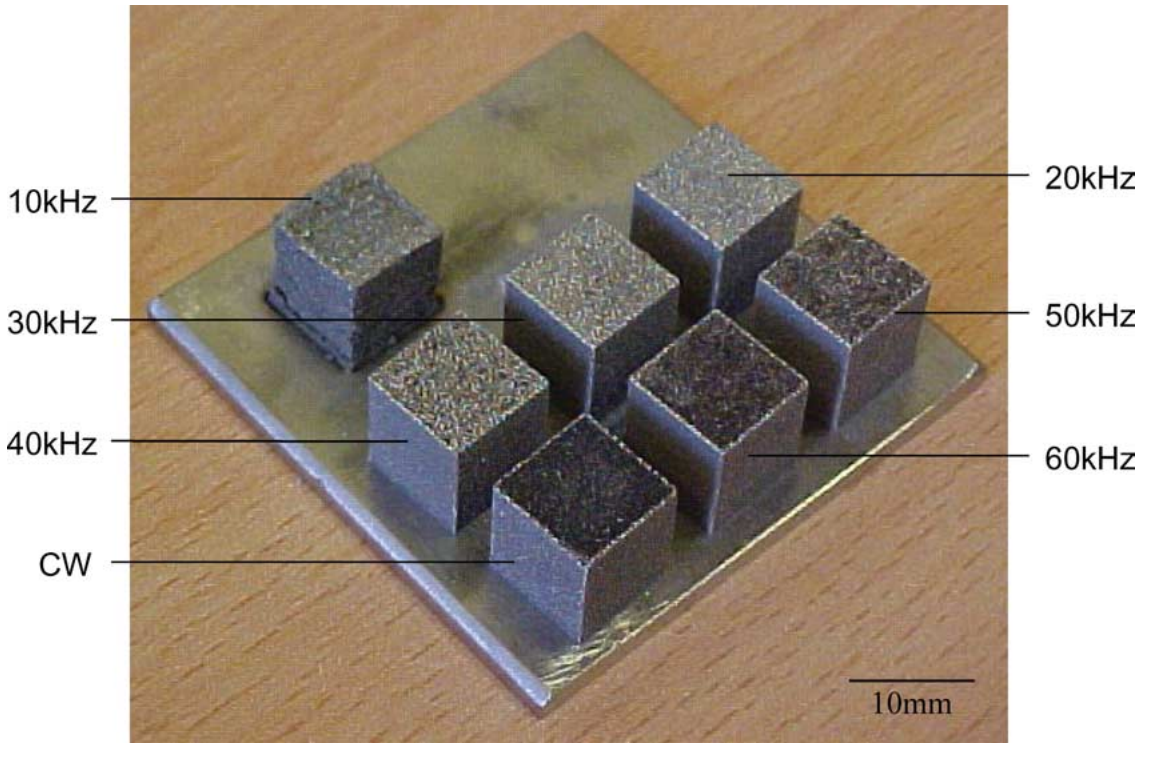

Figure 2 Array of 7 cubes produced in a single experimental run. Cubes are produced at varying laser pulse repetition frequencies (indicated) while laser scan speed and scan spacing remain constant.

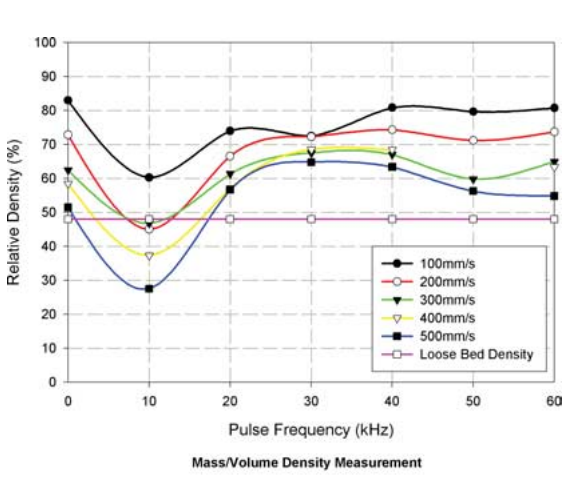

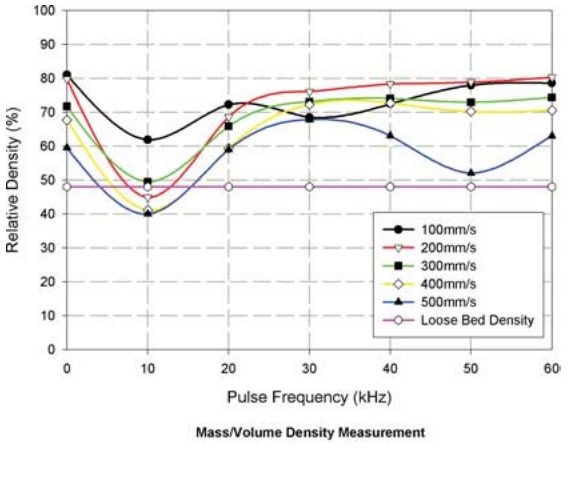

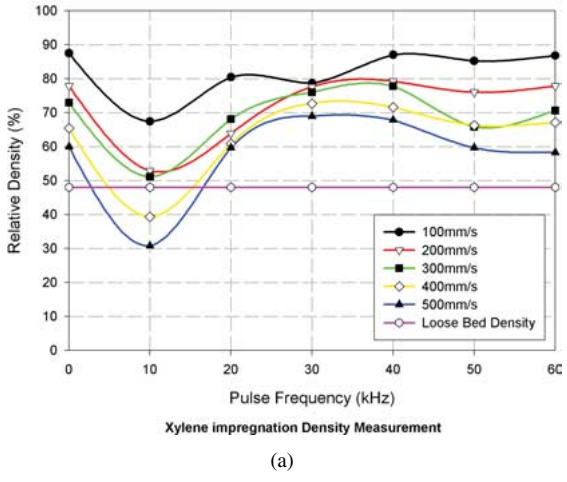

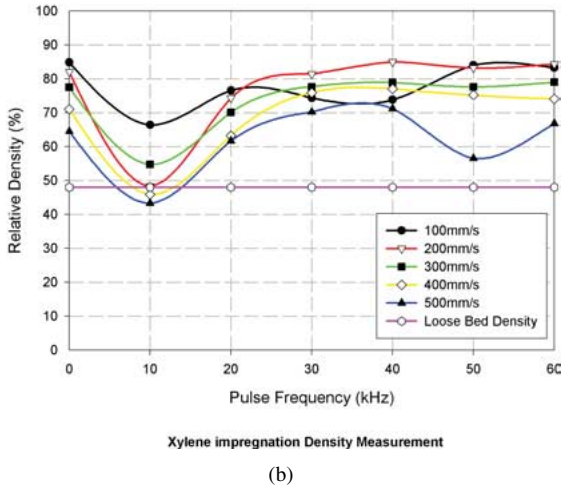

(a) (b)

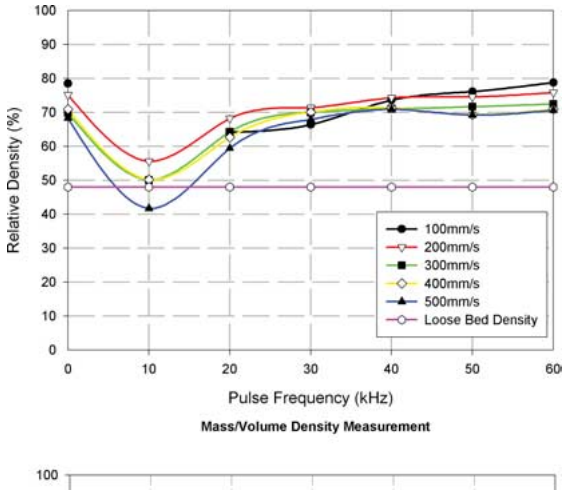

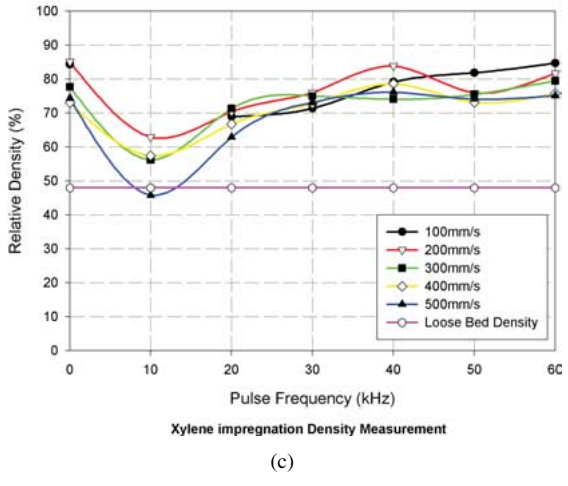

(c)

Figure 3 Material density as a function of laser pulse frequency and scan speed for various scan spacings: (a) 75 μm spacing, (b) 50 μm spacing and (c) 25 μm spacing.

below 20 kHz. At these low pulse frequencies, high peak powers are generated leading to plasma formation. The recoil compression associated with the plasma was observed to blast powder from the interaction site leaving little or no powder to be fused.

With increasing scan speed, in general the cubes exhibited lower densities. This is due to less incident energy per unit length resulting in less powder being consolidated into the melt bead and hence a higher porosity level. At the high scan speeds however, the effect of pulse frequency changes. In the PRF range 30–40 kHz, there was a clear increase in material density compared with the CW mode and 50–60 kHz range samples. Again, the material produced at 10–20 kHz showed low density, as low as 30%. This was substantially less than the original loose powder bed density at 48%.

The effect of scan spacing was less obvious. However, the results showed that samples fabricated with a larger scan spacing (75 μm) exhibited higher densities than those produced with small scan spacing (25 μm).

The characteristics of laser sintered or remelted material (layer thickness, strength, density) are often expressed in terms of the energy density applied during remelting. From Beaman *et al.* [10], this is described as:

$$E_\rho = \frac{P}{\pi r^2}\,\frac{2r}{v}\,\frac{2r}{s} \qquad (1)$$

where E_ρ = Energy density (Jmm^{-2}), P = laser power (W), r = beam radius (mm), v = scan velocity (mms^{-1}) and s = scan spacing (mm).

The first term relates to the laser intensity, the second term approximates the time a circle of radius r is exposed and the third term approximates the number of exposures received by any point on the material surface. When plotting the material density in terms of the energy density for individual variables, their influence becomes more apparent. The effect of PRF can clearly be seen in Fig. 4a.

Up to an energy density of approximately 7 Jmm^{-2}, the sample produced at the lowest frequency exhibits the highest density while the CW mode provides the lowest material density. At these low energy densities, the size of the melt bead generated by the laser is small and hence leads to high porosity. The recoil compression effects associated with the low pulse rates is substantial enough to deform the melt bead, forcing it from a circular shape to a flatter profile and hence improving layer density. Beyond 7 Jmm^{-2} the energy density is sufficient to produce larger melt beads which bond with one another to produce a high density layer. Under such conditions, the effect of recoil shock induced deformation is less of a contributing factor in achieving high material density.

The shape of the curve for each pulsing regime suggests a maximum energy density above which no increase in material density occurs. This is also true for the effect of scan spacing, shown in Fig. 4b. Here, material density is presented in terms of energy density for three scan spacings in CW mode. While the influence of scan spacing is not clear, the trend of increasing material density with increasing scan spacing is evident. Again, there appears a maximum energy density beyond which there is no increase in material density.

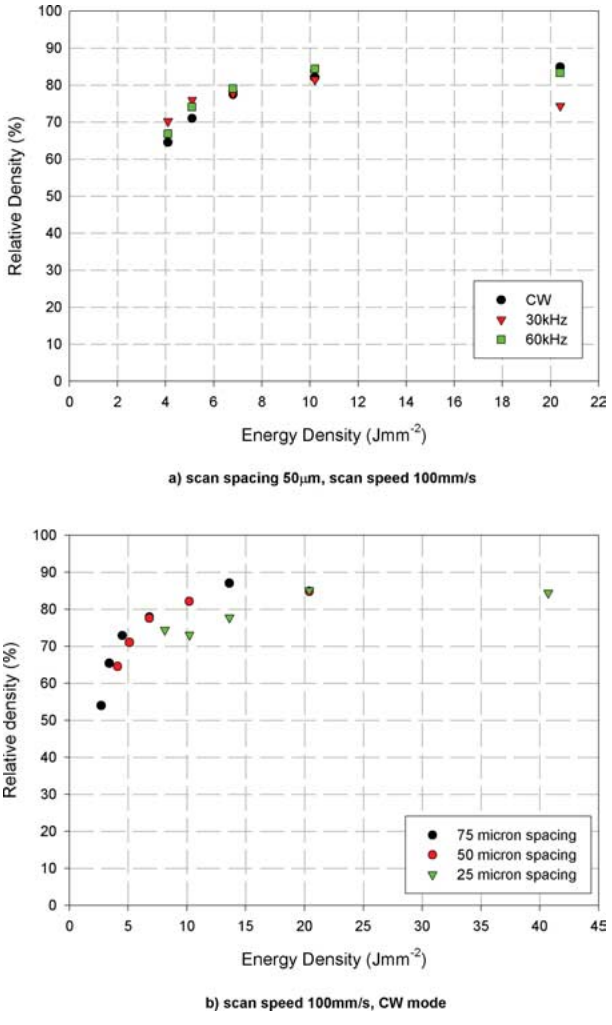

Figure 4 Material density as a function of energy density for: (a) variation in laser pulse frequency and (b) variation in scan spacing.

4.2. Optical analysis

Optical analysis of sample cross sections revealed a variety of porous structures across the laser scanning parameter range studied. Fig. 5 through 11 show sections views of the samples along the bi-directional scan direction (normal view) and through the scan direction (in-plane view).

In the CW lasing regime, the 75 μm scan spacing (25% beam overlap) sample (Fig. 5) shows extensive melting across several layers, in both the in plane and normal sections. Large areas of porosity also exist along single layers and across several layers. The section normal to the scan exhibits repeated angular porosity across many layers, while the porosity in the in-plane view is more horizontal and irregular. As the scan spacing is reduced to 50 μm (Fig. 6) the amount of porosity increases. The normal section exhibits an increase in the instance of angular porous structure and there appears a slight increase in the in-plane porosity. At 60 kHz PRF, this relationship between scan spacing and porosity is repeated (Figs 7 and 8).

At 500 mms^{-1} scan speed the samples exhibit significantly less material bonding (Figs 9 and 10). Though the

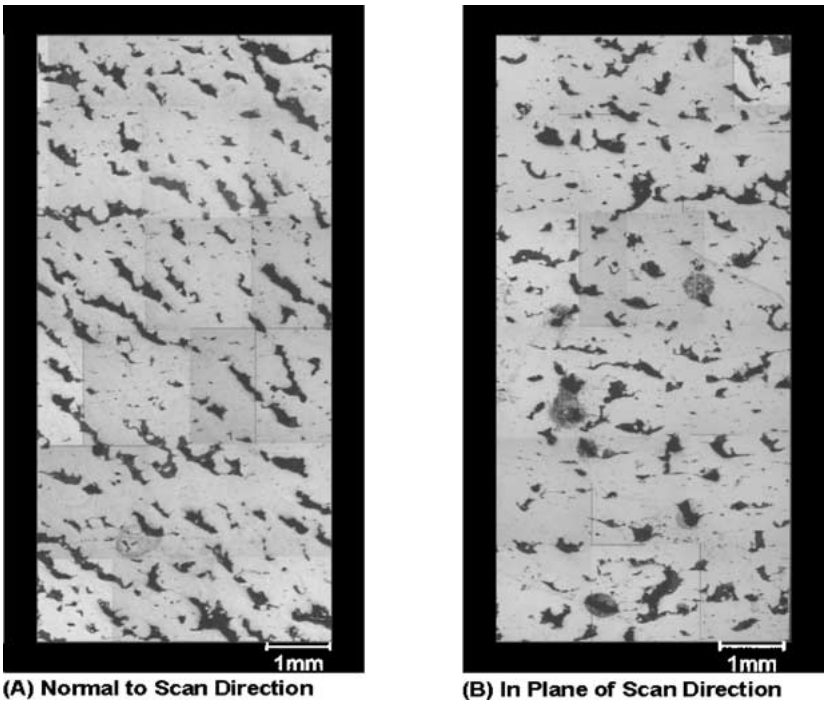

Figure 5 Cross section micrograph of cube produced at laser parameters: 80 W average laser power, CW mode, 100 mms^{-1} scan speed, 75 μm scan spacing.

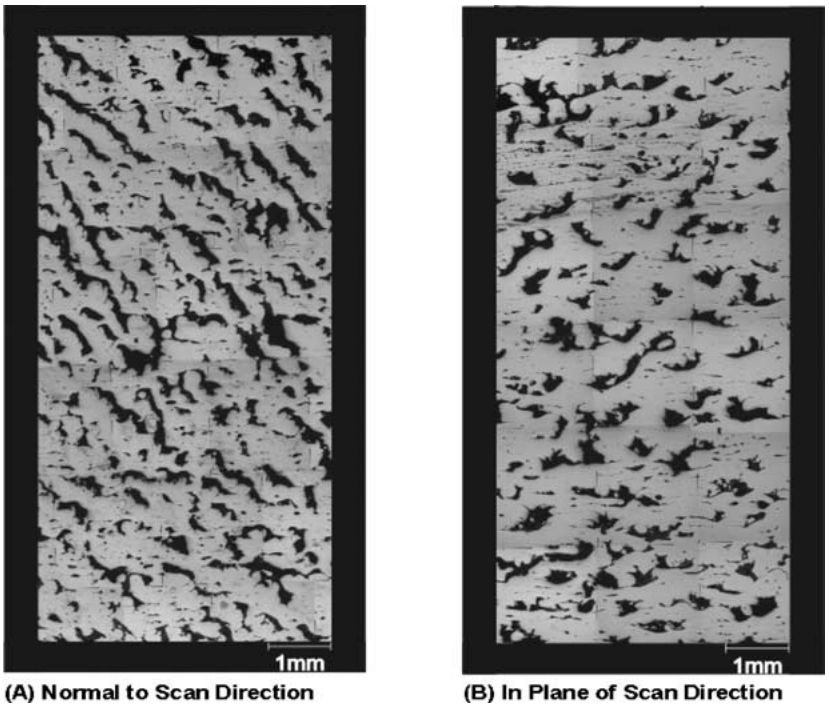

Figure 6 Cross section micrograph of cube produced at laser parameters: 80 W average laser power, CW mode, 100 mms^{-1} scan speed, 50 μm scan spacing.

densities are between 60–70%, the material is made up from small, resolidified melt beads with less connective bonding. The sample produced in the CW mode regime (Fig. 9) has a coarser structure than that exhibited by the 30 kHz sample (Fig. 10). The more rapid cooling of the melt associated with the low energy pulses with the pulsed laser interaction leads to the formation of finer melt beads, while the compression effects deform the beads leading to greater material density.

Fig. 11 shows the sections produced at 10 kHz pulse frequency. There appears to be very limited bonding between layers, but the material remains intact. The layers appear to be made up of long thin melt volumes in both section views, making the scan direction indeterminable.

5. Discussion

The study has demonstrated the successful production of cubic structures across a wide range of laser scanning parameters. The variation in laser scanning and pulsing parameters had a significant effect on the material

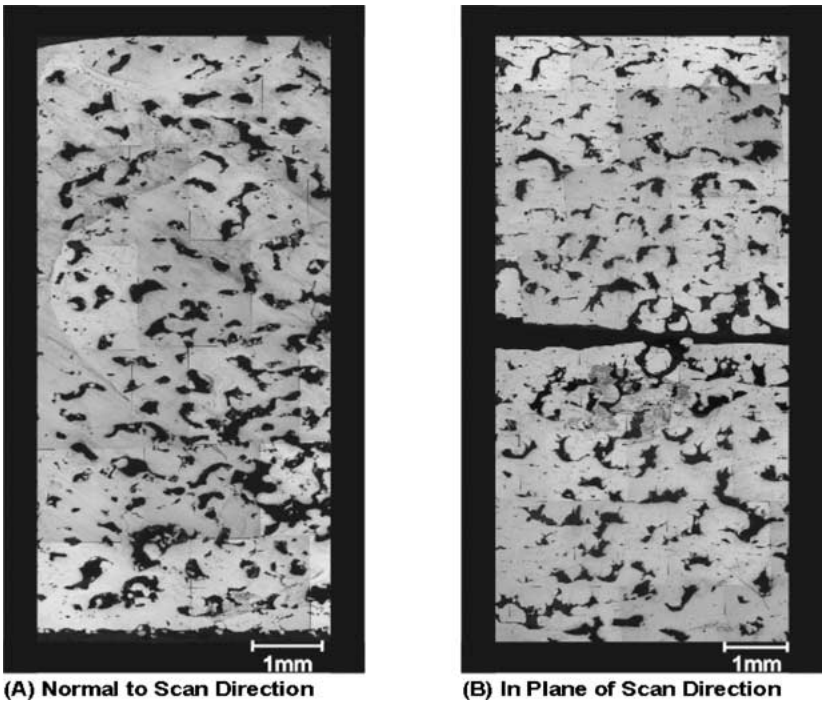

Figure 7 Cross section micrograph of cube produced at laser parameters: 80 W average laser power, 60 kHz Pulse Repetition Frequency, 100 mms^{-1} scan speed, 75 μm scan spacing (In plane section fractured during sample preparation).

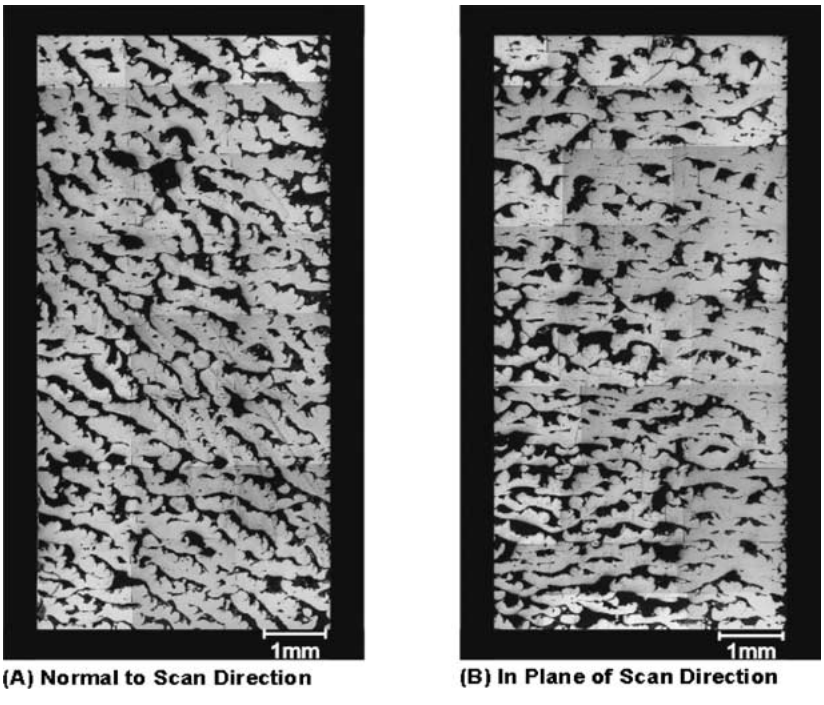

Figure 8 Cross section micrograph of cube produced at laser parameters: 80 W average laser power, 60 kHz Pulse Repetition Frequency, 100 mms^{-1} scan speed, 50 μm scan spacing.

density; samples exhibited a wide range of densities—between 30–87% of the theoretical density. The influence of the laser scanning parameters will now be discussed.

5.1. Effect of scan speed

The results clearly show a decrease in material density with increasing scan speed. At low scan speeds (100–200 mms^{-1}) the cubes exhibited the highest densities across the range of scan spacing. This is a result of the fact that there is a greater amount of energy delivered per unit length of a melt bead at slow scan speeds leading to more powder melting and larger beads. In this regime the cubes produced in CW mode and at high pulse frequencies (50–60 kHz) exhibited the highest densities achieved throughout the study. At the higher scan speeds the samples produced under CW and high frequency (50–60 kHz) pulse frequencies exhibited relatively low apparent density compared to those produced within the 30–40 kHz range. At high speeds energy input per unit length is reduced and therefore there is less powder melting leading to smaller beads. These beads are not large enough to consolidate into a

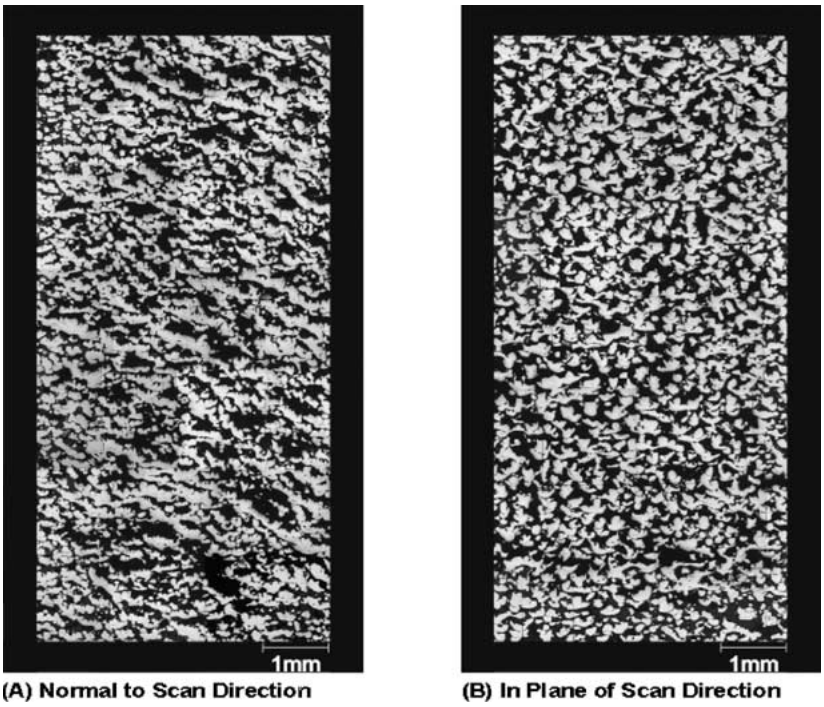

Figure 9 Cross section micrograph of cube produced at laser parameters: 80 W average laser power, CW mode, 500 mms^{-1} scan speed, 50 μm scan spacing.

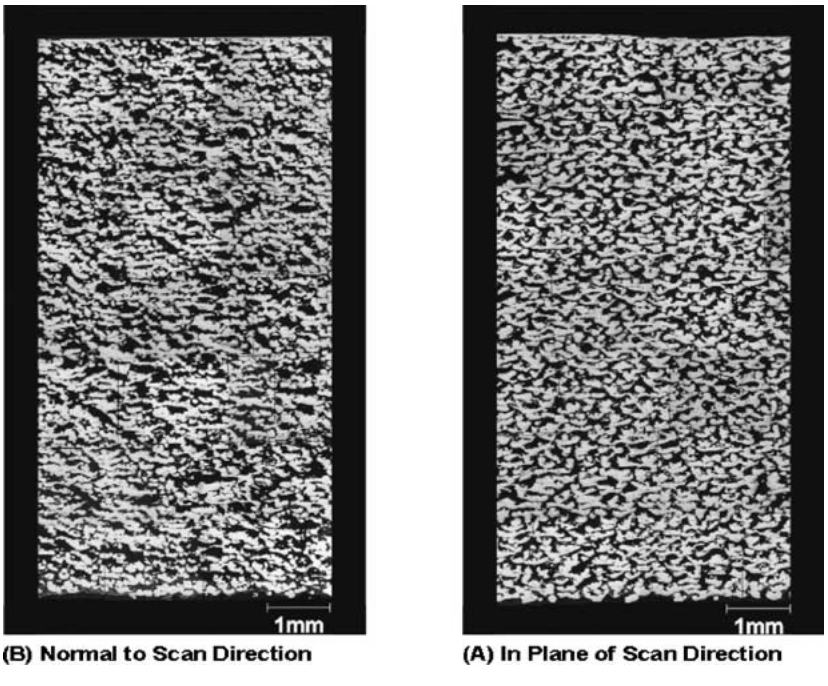

Figure 10 Cross section micrograph of cube produced at laser parameters: 80 W average laser power, 30 kHz Pulse Repetition Frequency, 500 mms^{-1} scan speed, 50 μm scan spacing.

dense layer. At the lower pulse rates (30–40 kHz) the recoil compression effect serves to deform the circular section beads into flatter shapes. This has the net effect of widening the melt beads and allowing adjacent beads to bond into a dense layer. The effect seen here correlates well with that seen in previous studies [5].

5.2. Effect of scan spacing

The scan spacing had a less significant effect on achieved material density than scan speed, however the general trend was that a higher scan spacing produces higher density material. Initial impressions may find this result peculiar, as one would assume a higher energy delivery would result in increased material density. However, it may be explained as follows: At low scan spacings the melt bead is exposed to multiple passes of the beam—the exact number depending on the degree of overlap. The result is that the bead is maintained at high temperature for long periods of time. Some portions of the bead will be solid, some semi-molten and some molten depending on the position of the laser. The melt volume of any bead is increased through radial conductivity into the powder bed and the capillary

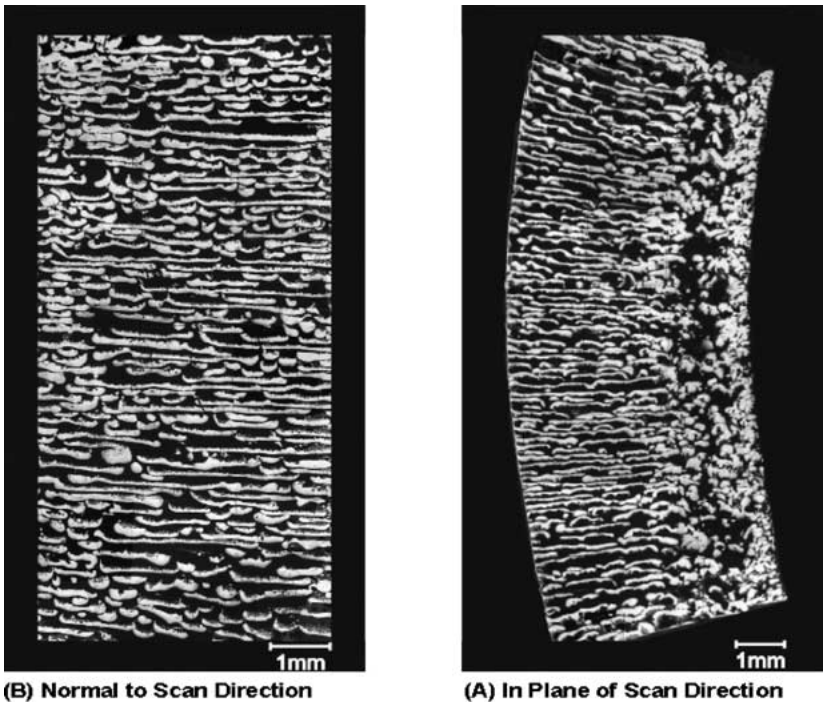

Figure 11 Cross section micrograph of cube produced at laser parameters: 80 W average laser power, 10 kHz Pulse Repetition Frequency, 500 mms^{-1} scan speed, 50 μm scan spacing. (In plane section is curved as a result of sample preparation).

forces associated with the wetting liquid. The greater the degree of overlap, the greater the time spent at high temperature, and the greater the degree of bead growth through powder incorporation. The presence of the substrate (or previously solidified layer) means there is a finite amount of powder available for consumption in the formation of a layer. The longer a bead is maintained at elevated temperature the more powder it consumes—leaving insufficient powder remaining for the formation of subsequent beads into a dense layer. Thus small scan spacings produce low density parts in multiple layer builds.

5.3. Influence of pulse frequency

In the low PRF range (10–20 kHz) extremely high peak powers are reached (approximately 20–40 kW) and a plasma is formed above the interaction site. During scanning of the initial 100 μm layer the explosive nature of the recoil compression was observed to blow all the powder away from the interaction zone, resulting in no bead formation. This occurred for all subsequent layers until a depth between 500–1000 μm was reached, at which point the volume of powder was sufficient to contain the effect. Beyond this point the explosive recoil compression drove the loose powder onto the substrate. This force, combined with the incident laser radiation, served to consolidate the powder and bond it to the substrate. The resulting densities of the samples produced in this PRF range were in certain cases, lower than the previously measured powder bed density. It is assumed that disturbance caused to the melt by the recoil compression shock was responsible for this phenomenon.

At higher pulse frequencies, lower peak powers were achieved and no plasma was formed and the recoil compression effect not observed. As pulse frequency increased the peak power decreased but the total energy delivered to the interaction site increased (due to more incident pulses per unit time). As a result more powder melting occurred at higher pulse frequencies leading to larger melt beads and higher material density. CW radiation may be approximated to infinitely fast pulsing and therefore would be expected to produce the highest density material. This theory is supported by the experimental results. In the 100–200 mms^{-1} scan speed regime the cubes produced in CW mode and at high pulse frequencies (50–60 kHz) did exhibit the highest densities achieved throughout the study.

However at faster scan speeds the greatest densities were achieved in the 30–40 kHz regime. In this range there was a recoil compression effect but it was not sufficiently violent to blow away loose powder. Instead it served to deform the normally circular section melt bead into a flatter shape. At the high scan speeds the melt bead width is not normally sufficient to allow adjacent beads to bond into a layer. However the induced deformation effectively widened the bead resulting in a higher density material.

5.4. Relevance of specific energy

The effect of laser pulse frequency can clearly be seen in Fig. 4a. Up to an energy density of approximately 7 Jmm^{-2} the lowest frequency provided the highest density and the CW provides lowest. This is to be expected because at low energy densities the size of the melt bead is small (leading to high porosity). The recoil effect associated with plasma formation at low pulse rates (high peak powers) deforms the small bead making it flatter and improving layer density. Beyond 7 Jmm^{-2} the energy density was sufficient to produce larger melt beads which bonded with one another to produce a dense layer. Under such processing conditions the effect of the recoil shock induced deformation

is less of a contributing factor in achieving high material density.

The shape of the curve for each laser pulsing regime (in Fig. 4a) suggests there is a maximum energy density above which no significant increase in material density occurs. This appears to be between 10 and 20 Jmm^{-2} but the exact point is unclear from the graph. The maximum material density achieved was approximately 87%. This also appeared to be the case for the analysis of scan spacing in terms of energy density. The curves in Fig. 4b appear to be approaching a maximum value of approximately 85% material density above an energy density of 15–20 Jmm^{-2}.

5.5. Optical analysis

Optical analysis provides further information about the structure of the consolidated material. The in-plane views generally showed a random occurrence of voids between layers, whereas the normal view revealed the periodic angular porosity through almost all samples. The shape of the melt across the layers is very similar to that observed by Kraupl [11]. More significantly, the angular shape resembles the surface formations observed in thin wall structures produced by this technique reported previously [12]. Such a surface structure is shown in Fig. 12.

The section views of the samples produced at high scan speeds (500 mms^{-1}) show a reduction in volume of melting. The volume of melt in the CW mode sample (Fig. 9) is greater than that of the pulsed sample (Fig. 10) which appears to have a structure that resolidified very quickly. The increased volume of melt in the CW sample may have resulted from surface tension forces drawing local material into the melt, thus leaving larger regions of porosity, while the low energy pulses of the 30 kHz sample provided limited thermal input while recoil effects acted to produce a tightly knit structure. The section views of the sample produced at 10 kHz (Fig. 11) suggest that due to the excessive peak intensities, the recoil pressures are substantially affecting the melt, thus leaving a highly porous structure with very little fusion between the layers. It is remarkable that the cubes produced at these pulse frequencies remain intact, particularly with densities as low as 30%.

From these results, it may be possible, with careful control of peak intensities, to tailor the laser processing parameters to provide a particular desired density in the component being produced. However, the high-density samples still exhibit an excessive amount of porosity to provide adequate mechanical properties for the fabrication of functional, load bearing components. Therefore, the causes of porosity must be addressed.

There is a possibility that the large range of particle diameters ($1\ \mu m < \phi > 50\ \mu m$) may be causing variations in the quantity of melting. The 100 μm beam diameter may only partially melt the larger 50 μm particles as it traverses the powder bed whilst vaporising the smaller $<1\ \mu$m particles. It may be concluded that a smaller distribution of powder sizes is required to negate this effect and lead to increased material density. Further, the powder bed density before processing should be taken into account. Measurements showed that the powder bed exhibits approximately 50% of the solid material density. Therefore there will be insufficient powder per unit volume to produce a high density material during the remelting of each layer.

The surface tension and Marangoni convective stirring forces acting to shape the melt towards a spherical or cylindrical profile will create areas of voiding between scans. The effect of surface tension will increase

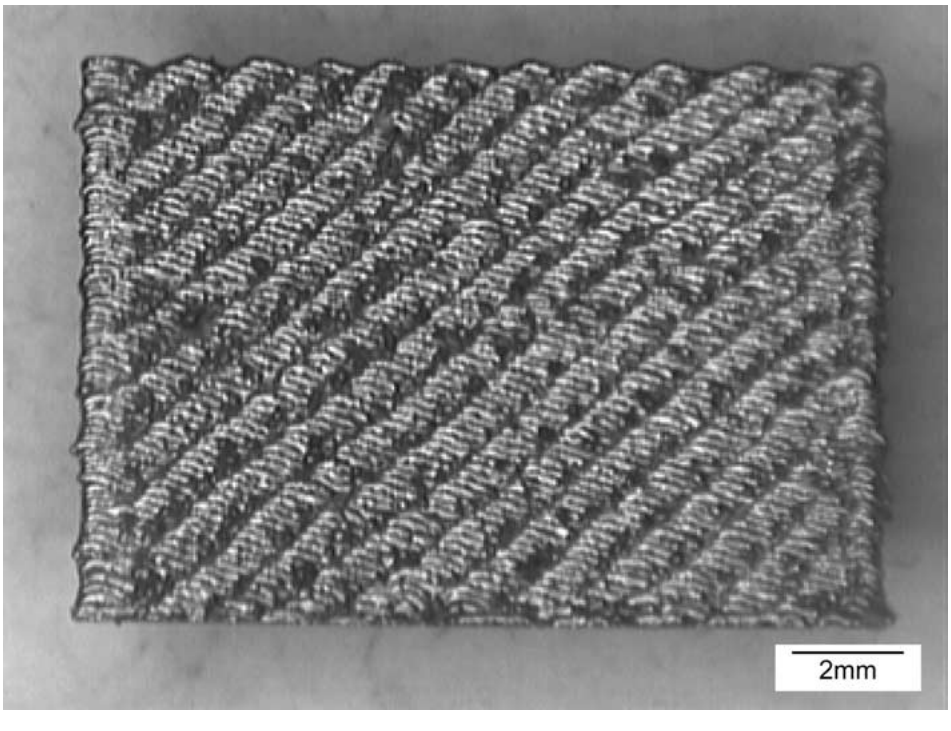

Figure 12 Surface structure present in thin wall sample. Periodic angular porosity within cubic samples may be attributed to the melt dynamics associated with this structure.

with poor wetting due to oxide formation on resolidified surfaces. While the chamber is under non-oxidising environment, there is likely to be oxygen trapped in the loose powder bed and oxygen partial pressures as low as 10^{-20} may still yield oxide formation during processing [13].

Clearly the most substantial cause of porosity in the samples however, appears to be the periodic angular porous structure throughout the material. The melt dynamics causing the surface structure in the thin wall sample shown in Fig. 12 are as yet unexplained. However, the formation of the structure may be eradicated by careful manipulation of the scanning laser over the powder layer. Thus it is concluded that a simple bi-directional rasterscan with optimised laser parameters will achieve limited success in producing high density material by the DMLR process. To this end, a scanning strategy has been developed to produce high density material and has been successfully implemented and is reported elsewhere [14].

6. Conclusions

This paper has examined the effects of laser process variables on the density of cubic primitives produced by the DMLR process. The results have shown interesting trends in the resulting material densities as functions of pulse frequency, scan speed and scan spacing.

A maximum material density of 87% of theoretical density was achieved at 100 mms^{-1}, 80 W and 75 μm scan spacing in the CW mode regime for a 100 μm beam diameter. Increasing scan speed resulted in a reduction of sample density, whereas increasing scan spacing improved density. Samples produced at 5-mms^{-1} scan speed failed due to the generation of excessive thermal stresses. At high scan speeds (400–500 mms^{-1}), the samples exhibiting the highest densities were produced with pulse frequencies in the range 30–40 kHz. This was due to low pulse energies generating limited melt volume while recoil compression forces (caused by plasma formation) modified melt pool shape before resolidification, resulting in a tight knit porous structure. At pulse frequencies in the range 10–20 kHz, the effects of recoil compression has resulted excessive modification of the melt, resulting in cube densities as low as 30%, almost 20% less than the loose powder bed density.

Optical analysis of the samples revealed an angular structure to the porosity along the beam direction which spanned many layers. The cause of this may be due to the melt dynamics, as observed in the formation of surface structures in thin wall samples.

When the sample densities were plotted against the energy density delivered across the powder layer, the material density appeared to tend towards a maximum at 15–20 Jmm^{-2}. Whilst it cannot be concluded that this is a definite process limit, it is assumed that simply increasing energy density is not an appropriate route to achieving material densities approaching 100%.

Acknowledgements

The authors would like to thank Mr. Lawrence Bailey for his invaluable contribution to the continued development of the research equipment. We would also like to thank the EPSRC for their support of the program through a ROPA award. The Manufacturing Science and Engineering Research Centre is funded by the EPSRC under the Innovative Manufacturing Research Centres program.

References

1. N. HOPKINSON and P. DICKENS, *Rapid Prototyping Journal* **7**(4) (2001).
2. K. W. DALGARNO, T. H. C. CHILDS, I. ROWNTREE and R. ROTHWELL, "Finite Element Analysis of Curl Development in the Selective Laser Sintering Process," Proc. Solid Freeform Fabrication Symposium (University of Texas at Austin, TX, 1996) Vol. 7.
3. W. M. STEEN, "Laser Material Processing" (Springer Verlag, 1991).
4. V. SVETSOV, M. POPOVA, V. RYBAKOV, V. ARTEMIEV and S. MEDVEDUK, *Shock Waves* **7** (1997).
5. R. MORGAN, C. J. SUTCLIFFE and W. O'NEILL, *Rapid Prototyping Journal* **7**(3) (2001).
6. "ASM Metals Reference Book," 3rd ed. (ASM International, Ohio, USA, 1993).
7. W. MEINERS, K. WISSENBACH and R. PROPAWE, "Direct Selective Laser Sintering of Steel Powder," Proc. Laser Assisted Net shape Engineering (LANE, 1997) Vol. 2.
8. S. KATAYAMA, N. SETO, M. MIZUTANI and A. MATSUNAWA, "Formation Mechanism of Porosity in High Power YAG Laser Welding," Proc. ICALEO 2000, Section C, p. 6.
9. G. ARTHUR, *J. Inst. Met.* **83** (1954–55) 329.
10. J. J. BEAMAN, J. W. BARLOW, D. L. BOURELL, R. H. CRAWFORD, H. L. MARCUS and K. P. MCALEA, "Solid Freeform Fabrication: A New Direction in Manufacturing" (Kluwer Academic Publishers, 1997).
11. S. KRAUPL and P. HOFFMAN, "New Developments for Laser Sintering of Metallic Powders," Proc. Laser Assisted Net Shape Engineering (LANE, 1997) Vol. 2.
12. R. H. MORGAN, A. PAPWORTH, C. J. SUTCLIFFE, P. FOX and W. O'NEILL, "Direct Metal Laser Re-Melting of 316L Stainless Steel Powder. Part 1: Analysis of Thin Wall Structures," Proc. Solid Freeform Fabrication Symposium (University of Texas at Austin, TX, 2001) Vol. 12.
13. R. M. GERMAN, "Sintering Theory and Practice" (Wiley Interscience Publications, 1994).
14. R. H. MORGAN, A. PAPWORTH, C. J. SUTCLIFFE, P. FOX and W. O'NEILL, *J. Mater. Sci.* **37**(15) (2002).

Received 29 May
and accepted 11 September 2003